

Dielectric relaxation in camphorsulfonic acid-doped polyaniline thin film

B. S. MISIRLIOĞLU^{a,*}, F. KARAMAN^b, V. UĞRASKAN^b, M. SERİN^a, Ö. YAZICI^b

^aDepartment of Physics, Yildiz Technical University, 34220 Istanbul, Turkey

^bDepartment of Chemistry, Yildiz Technical University, 34220 Istanbul, Turkey

Impedance spectroscopy and dc techniques were employed in order to investigate the relaxation mechanisms in drop casting film of camphorsulfonic acid-doped polyaniline. Both dc and ac conductivity measurements were performed between 298 K and 435 K. Based on the existing theories of ac conduction, it has been concluded that free band conduction is dominant mechanism in the sample. The impedance spectra of the sample displayed an electrode response at low frequency and a single high frequency semicircular arcs in the complex plane plot at all temperatures, with their centres lying below the real axis at a particular angle of depression indicating the distribution of relaxation times. It was found that both the real and imaginary parts of the complex dielectric function showed a saturation at higher frequencies and a strong dispersion at lower frequencies. The overall dielectric properties were mainly dominated by a Maxwell–Wagner type of relaxation with grains and the grain boundary.

(Received September 8, 2015; accepted October 28, 2015)

Keywords: Polyaniline, Camphorsulfonic acid, Dielectric, Conductivity, Impedance

1. Introduction

Intrinsically conducting polymers, as polyaniline, have attracted much attention because of their characteristic properties such as, stability in air, high intrinsic conductivity, electrochemical, and optical properties [1]. It has been reported that conducting polymers doped with poly-acids are especially interesting due to their high resistance to heat and water [2]. Another property that makes conducting polymers interesting is the fact that some of them are soluble in water and/or in organic solvents, which facilitates their application on surfaces as a thin film [3]. There are special properties of this class of compounds that make them suitable for applications in the field of molecular electronics such as, photovoltaic cells [4], organic light emitting diodes [5] and as the basis of sensor devices for environmental and industrial applications [6,7]. During the past three decades, there has been a growing interest in studying the properties of thin films based on conducting polymers. However, in order to estimate the full potential of these materials, a better understanding of the electrical properties of these compounds in the thin film form is crucial. Such studies on the d.c. and a.c. electrical behavior are capable of providing considerable insight into charge transport mechanisms and carrier trapping in these materials. Measurements of dc and ac conductivity is a reliable method to study the localized states near the band edges below the conduction and above the valance bands produced by the substitutional disorders which controls many of the opto-electronic properties. Hence, a study of dc and ac conductivity in these materials will throw light on the nature of these levels and have considerable importance owing to their potential application to opto-

electronic devices and sensor systems [8-14]. Dielectric, Schottky barrier diode and photovoltaic behaviour as a hole injection layer, have been studied in some detail by various workers in their doped, undoped and composite form [4,15,16,17]. However, little previous work has been performed on impedance spectroscopic investigation, most of this being confined to corrosion protection of poly acid doped polyaniline [2].

In this work we present the results of dc and impedance spectroscopic measurements performed on drop casting camphorsulfonic acid-doped polyaniline film and try to gain an understanding of the transport mechanism in this film by discussing in terms of existing theory.

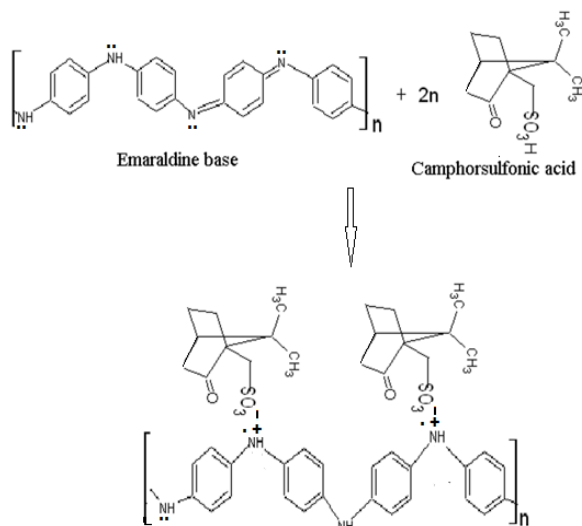
2. Experimental

2.1 Synthesis of camphorsulfonic acid-doped polyaniline

The HCl doped polyaniline emeraldine (PANI.HCl) was synthesized by oxidative polymerization of aniline with ammonium persulfate at room temperature. The mole ratio of oxidant to aniline was 1.25. Aniline (GPR Rectapur, >98.5%) was distilled under reduced pressure prior to use. 1.85 mL freshly distilled aniline was dissolved in 50 mL 1 M HCl (Merck) solution. 5.71 g ammonium persulfate (Sigma-Aldrich, 98+ %) was dissolved in 50 mL 1 M HCl solution. Both solutions were kept for 1 h at room temperature, then mixed in a beaker, briefly stirred, and left at rest to polymerize. Next day, the dark green polyaniline (PANI) precipitate was collected on a filter, washed three times with 100 mL portions of 0.2 M

HCl, and then three times with 100 mL portions of acetone. HCl doped polyaniline emeraldine (PANI.HCl) powder was obtained after being dried in air and then in vacuo at 60 °C for 24 h. The dried PANI.HCl powder was neutralized with 100 mL 0.5 M ammonium hydroxide (Sigma-Aldrich, 28.0-30.0 % NH₃) in ultrasonic bath for 1 h, filtered, washed with the deionized water until the filtrate was clear and colorless. The dark blue polyaniline emeraldine base (PANI.EB) was obtained after being dried in the vacuo at 60 °C for 24 h.

Then, camphor sulfonic acid doped polyaniline/poly(ethylene oxide) (PANI.CSA/PEO) blend was prepared by mixing in chloroform as described in the literature [18]. 100 mg PANI.EB was dissolved in 10 mL chloroform and then 129 mg±10-camphorsulfonic acid (TCI, >98 %) was added into the solution (Scheme-1). The solution was stirred for 6 h and filtered. Next, 10 mg PEO with a 400 000 g/mole was added, and the PANI.CSA/PEO blend solution stirred for 2 h. The sample was left in a bottle for 4 days and then filtered with a 220 nm millipore filter.



Scheme 1. Camphorsulfonic acid-doped polyaniline

2.2 Electrical characterisation of camphorsulfonic acid-doped polyaniline film:

The measurement electrodes used in the dc and ac conductivity measurements consist of an interdigital array of metal electrodes photolithographically patterned on pre-cleaned glass substrate. Glass substrates were thoroughly cleaned by ultrasonically and then coated with 150 Å of chromium followed by 1500 Å of gold in a Leybold Univex 450 coater system. The film patterned photolithographically and etched to provide 10 fingers pairs of electrodes having a width of 50 μm, spaced 50 μm from the adjacent electrodes. Thin film of PANI.CSA/PEO was prepared by drop-casting a concentrated solution of PANI.CSA/PEO in chloroform onto a interdigitated electrode structures. The film of PANI.CSA/PEO was dried at room temperature under ambient conditions for 24 h to evaporate the solvent. The substrate temperature was kept constant at 298 K during deposition of the materials over the electrodes. Dc conductivity measurements were performed between 298 K and 435 K by using a Keithley

617 electrometer. Impedance spectroscopy and ac conductivity measurements were carried out with a HP 4192A impedance analyzer in the frequency range, 5–13x10⁶ Hz, and in the temperature range from 298 K to 435 K. All the measurements were performed under 10⁻³ mbar and in the dark, but the values did not changed under illumination with the indoor lighting. The error in the measurement of the impedance spectra of the PANI.CSA/PEO film is estimated at about 3%. The impedance and dc conductivity data were recorded using an IEEE 488 data acquisition system incorporated to a personnel computer.

3. Results and Discussion

3.1. Dc and ac conductivity

The ac conductivity, $\sigma_{ac}(\omega)$, was measured during heating the sample from 298 K to 435 K. Fig. 1 shows the typical conductivity data as a function of frequency at various fixed temperatures. For the temperature > 364 K, a noticeable decrease in conductivity can be seen. Repeated measurements on the same sample reveals that the decrease in conductivity is not due to phase transition. The decrease in conductivity can be attributed to the oxygen and water content in the sample. As can be seen from the Fig. 1 that the observed ac conductivity patterns show a low frequency dispersion arising due to electrode polarization, frequency independent plateau in intermediate frequency region and high frequency dispersion. It is clear from Fig.1 that the conductivity spectrum remains similar as the temperature increases, except dispersion in the low frequency region at 435 K, where the deviation from the plateau region is declined. This behavior of ac conductivity obeys the universal power law [19], $\sigma_{ac}(\omega, T) = \sigma_0(0, T) + A\omega^s$, where $\sigma_0(0, T)$ is the dc conductivity (σ_{dc}), A and s have usually been found to be temperature dependent parameters. In the present work, dc conductivity $\sigma_0(0, T)$ has been extracted from the frequency-independent plateau of the $\log \sigma_{ac}(\omega, T)$ versus $\log(\omega)$ plots as well as calculated from the slope of the measured current voltage (I-V) characteristics by using the following relation

$$\sigma_{dc} = \frac{I}{V} \frac{t}{(2n-1)lh} \quad (1)$$

where I is the measured current, V is the applied voltage, t is the distance between the finger pair, n is the number of the finger pair, l is the overlap length and h is the thickness of the electrode. I-V measurements were carried out after films deposition and as the temperature was increased, so that conduction arising from impurity levels are not expected. It was observed that the measured conductivity for the film of the PANI.CSA/PEO depend exponentially on temperature such that the conductivity exhibits a variation of the form,

$$\sigma_{dc} = \sigma_0 \exp\left(-\frac{E_A}{kT}\right) \quad (2)$$

where E_A is the activation energy, T is the temperature, k is the Boltzmann's constant and σ_0 is the constant of proportionality. The activation energies for the sample was evaluated from the slopes of the $\ln(\sigma_0)$ versus $1/T$ graph and was found to be 0.24 eV.

In order to gain more insight into the frequency dependent conduction mechanism involved, various models such as quantum mechanical tunneling (QMT) and correlated barrier hopping (CBH) has been proposed, but it is not easy to decide which of those mechanisms is responsible for the observed conduction mechanism. It has previously been suggested [20] that the frequency exponent s parameter may give an idea about the charge transport mechanism in the system. Values of the frequency exponent s were calculated from the straight-line fits in $\ln\sigma_{ac}(\omega, T)$ versus $\ln(f)$ (inset of Fig.1). Our calculations showed that s is definitely a function of temperature and shows a general tendency to increase with increasing temperature till 316 K and then decreases.

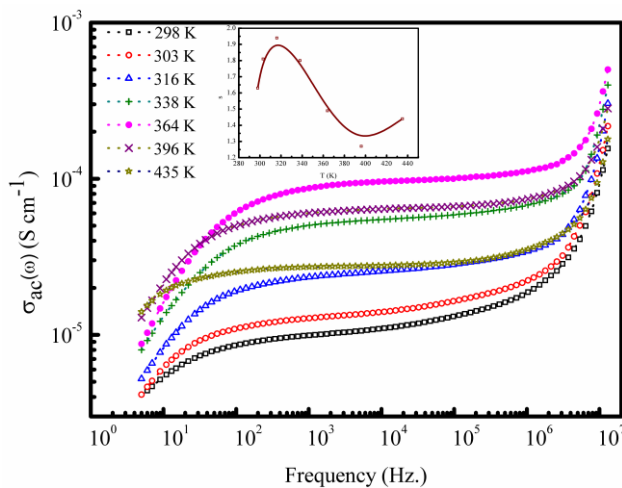


Fig. 1 Variation of ac conductivity, $\sigma_{ac}(\omega, T)$, with frequency at different temperatures

In QMT model which is based on the tunneling of an electron through a barrier separating two localized states near the Fermi level [21], the exponent s is temperature independent and has a constant value of 0.8. On the other hand, CBH model suggests a temperature dependent s parameter which is given by,

$$s = 1 - \frac{6kT}{W_{OB}} \quad (3)$$

where T is temperature, k is Boltzmann's constant and W_{OB} is the optical band gap. According to CBH model, in contrary to QMT model, the frequency exponent s temperature-dependent and increases with decreasing temperature. According to eq. (3), the s values should approach unity with increasing temperature. The comparison of the experimentally determined s values with the prediction of QMT and CBH models suggest that the dependence of exponent s on temperature can not be explained by neither the QMT model, nor the CBH model.

As can be seen from the inset of the Fig.1 that the extracted values of the frequency exponent s is always higher than unity. This behaviour of exponent s reveals a free band is the dominant conduction mechanism in PANI.CSA/PEO film.

3.2. Impedance study

The variation of real and imaginary parts of impedance, $Z(\omega) = R(\omega) + jX(\omega)$, as a function of frequency at various temperature for the film of PANI.CSA/PEO is presented in Fig. 2 (a) and (b), respectively. It becomes clear that there is a monotonic decrease in the real part of the impedance for the film at low frequencies. At higher frequency the value of $R(\omega)$ merges irrespective of temperature, which indicates the presence of space charge polarization. As the temperature rises, the value of $R(\omega)$ becomes less sensitive to frequency increase. For the temperature > 364 K, an increase in $R(\omega)$ with increasing temperature is clear, as in dc case. Both the high impedance value at lower frequencies and the high frequency behaviour of $R(\omega)$ clearly indicate the presence of space charge polarization. With the exception of the electrode effect at low frequencies, the imaginary part (loss spectrum) of the complex impedance increased with increase in frequency in all the temperature ranges studied here and exhibited a maximum before starts decreasing rapidly. It was also observed that the frequency at which maximum loss occurred, called the relaxation frequency, shifted to higher frequency regions as the temperature increased up to 364 K. The appearance of peak in the loss spectrum (>364 K) and maximum shifts to higher frequency with an increase in temperature suggests the existence of relaxation properties of the material. The asymmetric broadening of the peaks on increasing temperature confirms the electrical processes in the material with a spread of relaxation time [19]. The relaxation phenomenon in the material may be due to the presence of immobile species/electron at low temperature and defects/vacancies at higher temperature. Further, all the curves merge at higher frequency irrespective of temperature. The coincidence of the $Z''(\omega)$ values in the high frequency region at all the temperatures may be possibly an indication of the accumulation of space charges in the material [22].

The Nyquist plots (imaginary versus real part of impedance) for PANI.CSA/PEO with working temperature are displayed in Fig. 3. It can be seen from this figure that the plots drawn between imaginary and real parts of the impedance show an electrode response at low frequency and a single high frequency semicircular arcs whose their radius decreases with increase in temperature. The analysis of experimental data of this sample shows that when the temperature increases the semicircle are slightly depressed, indicating deviation from the Debye dispersion relationship, and their maximum shift to higher frequencies. In the case of a depressed semicircle in the impedance spectra the relaxation time is considered as a distribution of values, rather than a single relaxation time. The proper interpretation of the obtained impedance

spectra allowed us to determine the equivalent circuit of PANI.CSA/PEO thin film deposited on IDT patterned glass substrate composed by a resistor (R_0) in parallel with a constant phase element (CPE) in series with another resistor (R_∞).

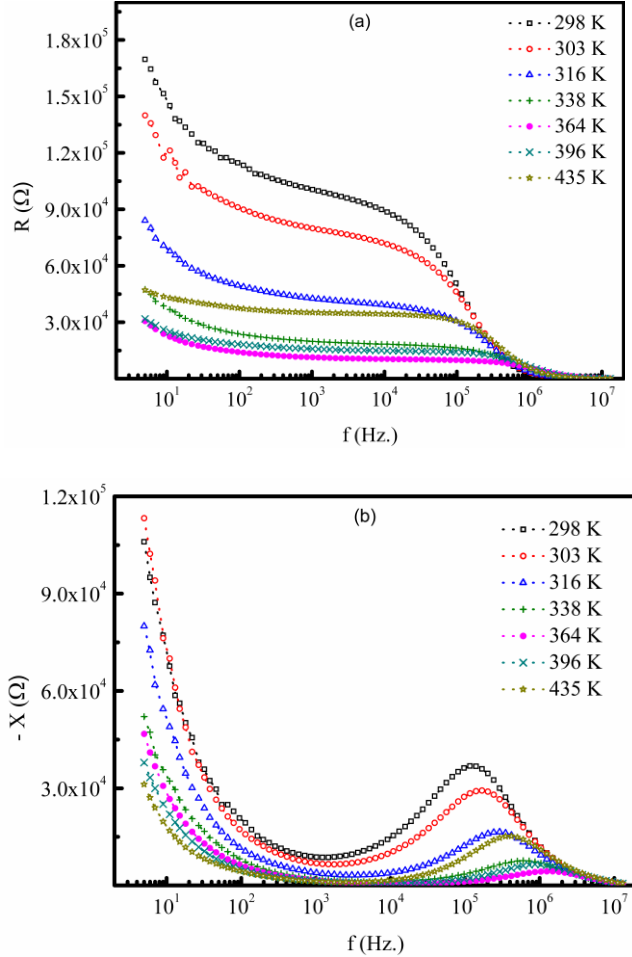


Fig.2 Frequency dependence of the real (a) and imaginary (b) parts of the impedance at the indicated temperatures.

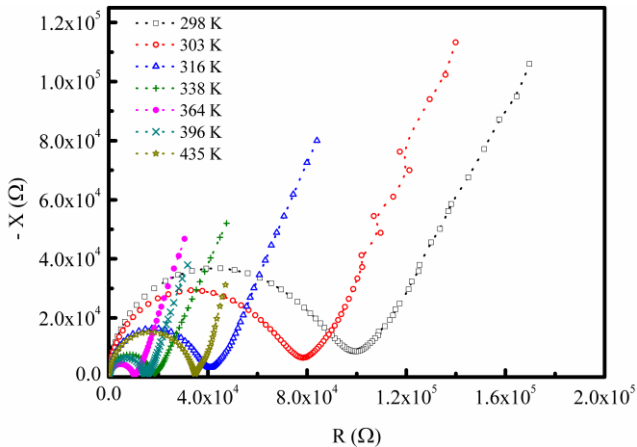


Fig.3 Nyquist plot (X vs. R) of the PANI.CSA/PEO sample at indicated temperatures

R_∞ and R_0 represent the resistance at $\omega \rightarrow \infty$ and $\omega \rightarrow 0$, respectively. In another word, the series resistance (R_∞) in the equivalent circuit represents the ohmic losses in the test fixture and electrode sheet resistance. The parallel resistance is of the coating material in parallel with that of the substrate. The presence of the constant phase element represents a slight distribution of relaxation times instead of a discrete relaxation time.

The components of the complex dielectric function, $\epsilon^*(\omega) = \epsilon'(\omega) - j\epsilon''(\omega)$, were obtained from the measured impedance spectra using the expression [23],

$$\epsilon^* = \frac{1}{j\omega C_0 Z^*} \quad (4)$$

where Z^* is the measured impedance, C_0 is the capacitance of the empty measuring cell and ω is the angular frequency of the applied signal. The relation between the real part and the imaginary part of the complex dielectric function defined as loss tangent ($\tan\delta = \epsilon''(\omega)/\epsilon'(\omega)$). Fig. 4 represents the dispersion curves of relative dielectric permittivity, $\epsilon'(\omega)$, at different temperatures. A strong frequency dispersion, $\epsilon'(\omega)$ decrease with increase in frequency, of permittivity is observed in the low frequency region followed by a nearly frequency independent behavior above ~ 100 Hz. It is also clear from Fig. 4 that the temperature dependence of $\epsilon'(\omega)$ is weak for higher frequencies. On the other hand, it exhibits a relatively strong temperature dependence in the low frequency region. An increase in $\epsilon'(\omega)$ with temperature may be attributed to the electric field which is accompanied by the applied frequencies. Such fields cause some ordering inside the samples as well as the formation of an electric moment in the entire volume of the film and in each separate polarizing molecule. When the temperature rises, the dipole orientation is facilitated, and this increases the dielectric permittivity. The decrease of $\epsilon'(\omega)$ with increase in frequency may be attributed to the electrical relaxation processes. The total polarizability of a material medium is mainly due to the contribution of deformational polarization (electronic and ionic) and relaxation polarization (orientational and interfacial). The various polarizabilities may be segregated from each other because each contribution has its own characteristic features which distinguishes it from the others. The frequency dependence of $\epsilon'(\omega)$ can be explained as follows: According to the Koops's [24] theory, which is based on the Maxwell-Wagner model, a solid is assumed to be composed of well conducting grains separated by highly resistive thin layers, grain boundaries. As a consequence of the applied signal to the sample, a space charge polarization is built up at the grain boundaries. The induced space charge polarization is controlled by the available free charges on the grain boundary and the conductivity of the sample. According to this model, the main contribution to the dielectric constant at low frequencies comes from the grain boundaries, which have a high dielectric constant. On the other hand, at high frequencies, the dielectric behaviour of the sample

is dominated by the grains which have a small dielectric constant.

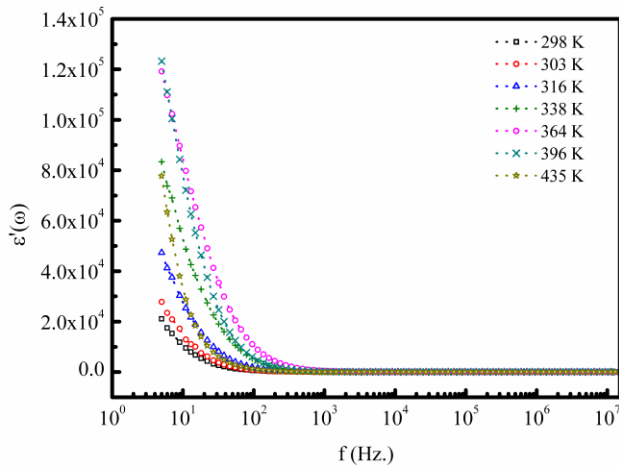


Fig.4 Frequency dependence of relative permittivity for PANI.CSA/PEO at indicated temperatures.

There is an additional aspect that should be recognized and accounted for in the interpretation of the frequency dependence of $\epsilon'(\omega)$. At low frequencies, the dipoles align themselves along the field direction and fully contribute to the total polarization. As the frequency is increased, the variation in the field becomes too rapid for the molecular dipoles to follow, so that their contribution to the polarization becomes less with a measurable lag because of internal frictional forces. The decrease of $\epsilon'(\omega)$ with the increase in frequency may be attributed to the electrical relaxation processes.

The imaginary components, $\epsilon''(\omega)$, of the dielectric function for the same film of PANI.CSA/PEO in the same frequency and temperature ranges were also investigated. Fig. 5 shows the frequency dependence of $\epsilon''(\omega)$ at different temperatures. As clearly seen from Fig. 5, no indication of a maximum peak is observed in $\epsilon''(\omega)$ in the region of frequency dependence. Fig. 5 illustrates that $\epsilon''(\omega)$ exhibits strong frequency dependence at higher temperatures and lower frequencies. At higher frequencies, the imaginary part of permittivity became less sensitive to both frequency and temperature. In the low frequency region, which corresponds to high resistivity due to the dominant effect of the grain boundaries at lower frequencies, more energy is required for transition of charge carriers between the levels. Therefore the energy loss is high at lower frequencies. In the high frequency region, the required energy for electron transfer between the levels is small and hence the energy loss is small.

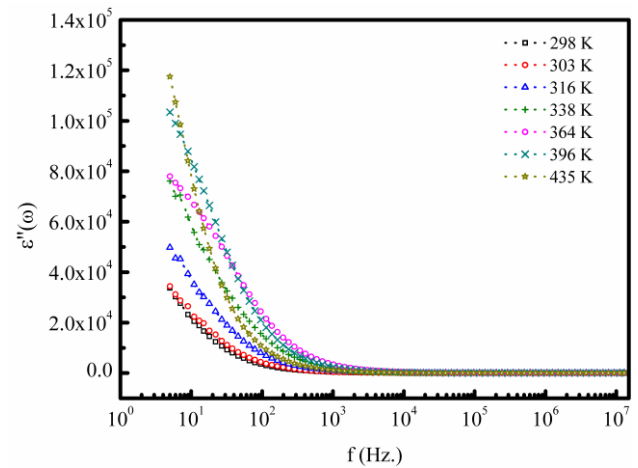


Fig.5 Variation of dielectric loss, $\epsilon''(\omega)$, with frequency at various temperatures.

The inverse frequency dependence of the dielectric loss at low frequencies was a confirmation of the non-Debye type character of the overall relaxation [25]. According to Stevels [26], the origins of the dielectric loss are conduction losses, dipole losses, and vibrational losses. As the temperature increases, the electrical conduction loss increases which increases the dielectric loss $\epsilon''(\omega)$.

4. Conclusions

In this study, camphorsulfonic acid-doped polyaniline was successfully synthesized, and dc, ac behaviour investigated in the first time. For this purpose, impedance spectroscopy measurements have been carried out on thin film of camphorsulfonic acid-doped polyaniline coated interdigital electrodes. The measurements covered the temperature range of 298–435 K and frequency range of 5 Hz to 13 MHz. It was found that the impedance spectra show strong temperature dependence in the investigated temperature and frequency ranges. The dielectric constant ϵ' and the dielectric loss ϵ'' were found to decrease with increasing frequency and increase with increasing temperature. Our analysis based on the existing theories showed that free band conduction is the dominant mechanism in the camphorsulfonic acid-doped polyaniline. It is also was observed that the overall dielectric properties were mainly dominated by a Maxwell–Wagner type of relaxation with grains and the grain boundary.

Acknowledgement

This work was supported by the Yıldız Technical University Commission of Scientific Research Projects under Grant No. 2012-01-01-GEP01. Authors are thankful to the Scientific Research Commission of Yıldız Technical University.

References

- [1] M. Diarmid, A.G. Kaner, R.B. In, Handbook of Conducting Polymers; Skotheim, T. A., Ed.; Marcel Dekker: New York, Vol. 1, pp. 718 (1986).
- [2] M.A.S. Oliveira, J.J. Moraes, R. Faez, Progress in Organic Coatings 65, 348 (2009).
- [3] R. Racicot, R. Brown, S.C. Yang, Synthetic Metals 85, 1263 (1997).
- [4] H. Bejbouji, L. Vignau, J.L. Miane, M.T. Dang, E.M. Oualim, M. Harmouchi, A. Mouhsen, Solar Energy Materials & Solar Cells 94, 176 (2010).
- [5] A. Drury, S. Chaure, M. Kröll, V. Nicolosi, N. Chaure, W.J. Blau, Chem. Mater. 19, 4252 (2007).
- [6] T.C.D. Doan, R. Ramaneti, J. Baggerman, J.F. van der Bent, A.T.M. Marcelis, H.D. Tong, C.J.M. van Rijn, Sensors and Actuators B 168, 123 (2012).
- [7] H.M. Hussien, M.H. Shinen, Chemistry and Materials Research 3(5), 61 (2013).
- [8] A.W. Marsman, C.M. Hart, G.H. Gelinck, T.C.T. Geuns, D.M. de Leeuw, J. Mater. Res. 19, 2057 (2004).
- [9] A.Z. Sadek, C.O. Baker, D.A. Powell, W. Wlodarski, R.B. Kaner, K. Kalantar-zadeh, IEEE Sensors Journal 7(2), 213 (2007).
- [10] S. Virji, R.B. Kaner, B.H. Weiller, J. Phys. Chem. B 110, 22266 (2006).
- [11] S.E. Bourdo, V. Saini, J. Piron, I. Al-Brahim, C. Boyer, J. Rioux, V. Bairy, A.S. Biris, T. Viswanathan, ACS Applied Materials and Interfaces 4(1), 363 (2014).
- [12] B.T. Raut, M.A. Chougule, A.A. Ghanwat, R.C. Pawar, C.S. Lee, V.B. Patil, J. Mater. Sci: Mater Electron 23, 2104 (2012).
- [13] S. Peng, P. Zhu, Y. Wu, S.G. Mhaisalkar, S. Ramakrishna, RSC Advances 2, 652 (2012).
- [14] T.H. Lim, K.W. Oh, S.H. Kim, Solar Energy Materials & Solar Cells 101, 232 (2012).
- [15] J. Lu, K.S. Moon, B.K. Kim, C.P. Wong, Polymer 48, 1510 (2007).
- [16] R. K. Gupta, R.A. Singh, Journal of Polymer Research 11, 269 (2004).
- [17] P.C. Ramamurthy, W.R. Harrell, R.V. Gregory, B. Sadanadan, A.M. Rao, Polymer Engineering and Science 44(1), 28 (2004).
- [18] M.J. Díaz-de León, Proceeding of The National Conference on Undergraduate Research (NCUR) 2001, Lexington, Kentucky, 2001.
- [19] A. K. Jonscher, Nature 267, 673 (1977).
- [20] A. Yazıcı, B. Sarıççek, A. Altındal, B. Salih, Ö. Bekaroğlu, Inorganica Chimica Acta 428, 83 (2015).
- [21] M. Pollak, Philos. Mag. 23(183), 519 (1971).
- [22] J. Plochanski, W. Wiczczonek, Solid State Ionics 28–30(2), 979 (1988).
- [23] E. Barsoukov, J. R. Macdonald, Impedance Spectroscopy, Theory, Experiment, and Applications, second ed., A. John Wiley & Sons, New Jersey (2005)
- [24] C. Koops, Phys. Rev. 83, 121 (1951).
- [25] A. Yazıcı, N. Ünüş, A. Altındal, B. Salih, Ö. Bekaroğlu, Dalton Trans. 41, 3773 (2012).
- [26] J. M. Stevels, in Handbuch der Physik, ed. S. Flugge, Springer, Berlin (1957).

*Corresponding author: sungubanu@gmail.com,
banu@yildiz.edu.tr